Publishing House
AKAPIT

**COMPUTER METHODS IN MATERIALS SCIENCE**

Informatyka w Technologii Materiałów

**Vol. 10, 2010, No. 4**

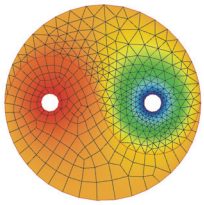

# NUMERICAL SIMULATION OF BLADE-OVER-ROLL COATING FORMING FLOWS

**EVAN MITSOULIS*, GEORGE ATHANASOPOULOS**

*School of Mining Engineering and Metallurgy,*
*National Technical University of Athens,*
*Zografou 157 80, Athens, Greece*
**Corresponding author: mitsouli@metal.ntua.gr*

**Abstract**

Numerical simulations have been carried out via the finite element method (FEM) for the forming flow of coating using a system of blade and roll. The flow domain encompasses both the coating fluid reservoir and the doctor-blade region with free surface and is fully two-dimensional. The materials of this study are Newtonian and shear-thinning polymer solutions used previously in an experimental and theoretical investigation. The pseudoplasticity of the polymeric liquids is modelled by the Carreau model, which fits well experimental data for the shear viscosities. For different roll speeds, the entire flow domain is analyzed, and the extent and shape of recirculating zones are found. Large vortices appear in the reservoir, and their intensity is computed under different operating conditions and blade geometries. The computed free surface profiles and coating thicknesses are in close agreement with the experimental ones. Shear thinning increases the coating thickness for a given geometry, as was also found experimentally, when compared with the Newtonian values. This increase is valid up to power-law index $n > 0.3$, while extreme shear-thinning (power-law index $n < 0.3$) reduces the coating thickness. This new finding is in agreement with previous findings in other geometries for highly shear-thinning fluids. The vortex decreases in size and intensity monotonically and linearly with n, in the range $1 \geq n > 0$. The simulations also provide a wealth of information regarding stresses and pressures and show that some geometries are better than others in coating operations. The flow geometry provides an interesting case for simulation and design, due to a combination of fluid mechanics and shear-thinning phenomena that take place in this flow field.

**Key words**: coating flows, blade-and-roll coating, carreau constitutive equation, shear thinning, vortex development

## 1. INTRODUCTION

Coating flows are of particular interest in the film coating industry, where minute volumes of liquid are coated on extremely thin layers over a substrate. The analysis so far has been based mostly on Newtonian (Kistler & Scriven, 1984) or generalized Newtonian models (Sullivan et al., 1987), which do not take into account the viscoelasticity of many coating liquids. The problem is compounded by the presence of free surfaces both upstream of the substrate and downstream, where the actual coating takes place (see figure 1a for the blade-coating process).

Previous experimental work by Sullivan and Middleman (1986) showed that rheological effects are important in blade coating, and in particular that viscoelasticity can have an influence in the flow patterns and affect the coating thickness of the liquids. The subject of properly modelling viscoelasticity through constitutive equations is a major one (Sullivan, 1986; Mitsoulis, 1990). Some efforts in

 ISSN 1641-8581

using realistic viscoelastic models, in particular integral constitutive equations of the K-BKZ type, have been made in the numerical simulation of coating flows (see, e.g., Mitsoulis & Triantafillopoulos, 1997; Mitsoulis & Pham, 1996), but the subject still needs a lot of additional work due to the inherent difficulties of coating flows.

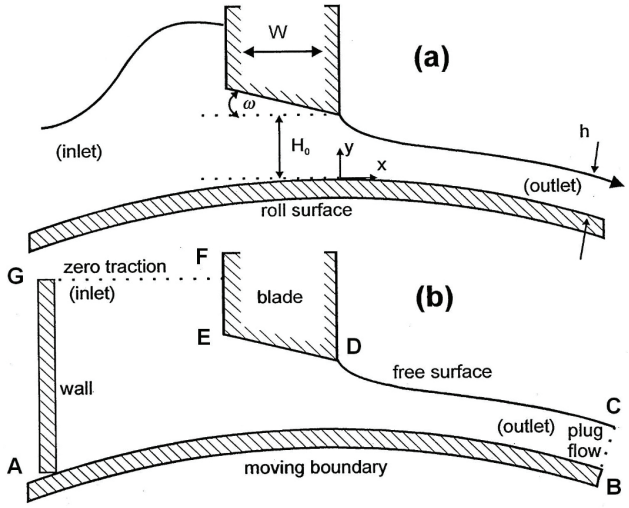


***Fig. 1.*** *(a) Schematic diagram of the blade-coating domain with relevant notation; (b) flow domain with the addition of a reservoir wall upstream and relevant boundary conditions.*

On the other hand, a lot of insight can be had by using shear-thinning constitutive laws and finding out the effect that shear thinning has on the upstream kinematics (vortex formation) and the coating thickness. This comes from the fact that many coating fluids are shear-thinning polymer solutions (Sullivan & Middleman, 1986; Sullivan, 1986). The previous work by Sullivan et al. (1987) showed some interesting features of blade-coating operations, but admittedly the boundary conditions used by the authors in the upstream reservoir were arbitrary and needed improvement. In particular, the upstream free surface is substituted by a reservoir wall in the present study (see figure 1b) in order to have a distinct boundary for the flow domain.

It is the purpose of this work to re-examine the geometries used in the experiments by Sullivan (1986) and give a full account of the upstream kinematics and coating thicknesses for shear-thinning polymer solutions. A parametric study of shear-thinning will be also carried out to find the effect that shear-thinning has on the flow behaviour and coating thickness.

## 2. MATHEMATICAL MODELLING OF COATING FLOWS

### 2.1. Conservation and constitutive equations

The coating flow between a moving substrate and a doctor blade for incompressible fluids (such as polymer solutions) under steady-state isothermal conditions is governed by the usual conservation equations of mass and momentum (Sullivan et al., 1987), i.e.,

$$\nabla \cdot \mathbf{v} = 0 \tag{1}$$

$$\rho \mathbf{v} \cdot \nabla \mathbf{v} = -\nabla p + \nabla \cdot \boldsymbol{\tau} \tag{2}$$

where $\mathbf{v}$ is the velocity vector, p is the scalar pressure, $\boldsymbol{\tau}$ is the extra stress tensor, and $\rho$ is the density.

The constitutive equation that relates the stresses $\boldsymbol{\tau}$ to the velocity gradients is the generalized Newtonian model (Sullivan, 1986) and is written as:

$$\boldsymbol{\tau} = \eta(\dot{\gamma})\dot{\boldsymbol{\gamma}} \tag{3}$$

where $\dot{\boldsymbol{\gamma}} = \nabla \mathbf{v} + \nabla \mathbf{v}^T$ is the rate-of-strain tensor and $\eta(\dot{\gamma})$ is the apparent viscosity given by the Carreau model

$$\eta(\dot{\gamma}) = \eta_\infty + \eta_0 \left[1 + (\lambda\dot{\gamma})^2\right]^{\frac{n-1}{2}} \tag{4}$$

In the above, $\eta_o$ is the zero-shear-rate viscosity, $\eta_\infty$ is the infinite-shear-rate viscosity, $\lambda$ is a characteristic time and $n$ is the power-law index. The magnitude $\dot{\gamma}$ of the rate-of-strain tensor is given by

$$\dot{\gamma} = \sqrt{\frac{1}{2} I_{\dot{\gamma}}} = \sqrt{\frac{1}{2}(\dot{\gamma} : \dot{\gamma})} \tag{5}$$

where $I_{\dot{\gamma}}$ is the second invariant of the rate-of-strain tensor.

The materials in question are Newtonian fluids and shear-thinning polymer solutions used in the previous experimental study by Sullivan and Middleman (1986). The polymer solutions are carboxymethyl-cellulose (CMC) solutions (1.25% wt) in distilled water. As such they are inelastic, shear-thinning. The values of the constants are given in table 1. With these values the predictions for the shear viscosity $\eta_S$ are plotted in figure 2, together with the experimental data.



***Table 1.*** *Material parameter values used in eq. (4) for fitting data of the 1.25% aqueous CMC polymer solution according to Sullivan (1986) ($\rho$ = 1.0 g/cm$^3$). For the Newtonian fluid (Karo Syrup), $\mu$ = 1.0 Pa·s and $\rho$ = 1.3 g/cm$^3$.*

| $\eta_o$ (Pa·s) | $\eta_\infty$ (Pa·s) | $\lambda$ (s) | n (-) |
|---|---|---|---|
| 1.7 | 0.017 | 0.22 | 0.52 |

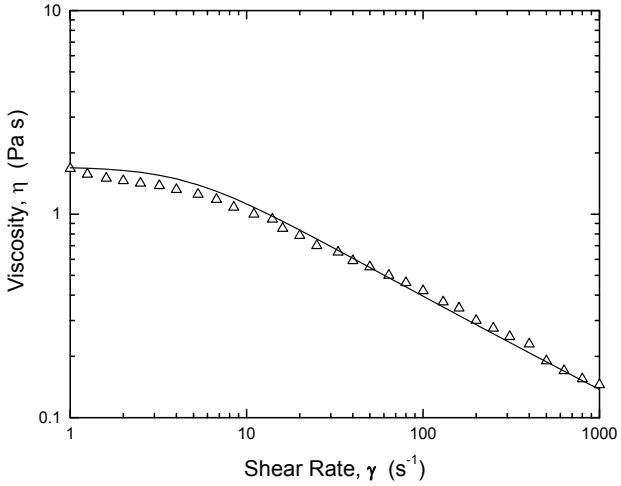


***Fig. 2.*** *Model predictions (line) of shear viscosity $\eta_S$ for the shear-thinning 1.25% CMC aqueous polymer solution using eq. (4) with the material parameters given in Table 1. Symbols are experimental data reported by Sullivan (1986).*

### 2.2. Boundary conditions

For the flow boundary conditions and with regard to figure 1b, we impose the following: (1) along the roll surface AB, which is a moving boundary, no-slip velocity, i.e., $v_t = V_R$, $v_n = 0$; (2) along the outlet exit BC, where a plug flow exists, zero surface tractions and $v_n = 0$; (3) along the free coating surface CD, a kinematic boundary condition of no-cross flow, i.e., $\mathbf{n} \cdot \mathbf{v} = 0$, where $\mathbf{n}$ is the unit outward normal vector to the surface; (4) along the blade wall DE, no slip velocity, i.e., $v_x = v_y = 0$; (5) along the vertical blade wall EF, no slip velocity, i.e., $v_x = v_y = 0$; (6) along the reservoir inlet entry FG, zero surface tractions and $v_x = 0$; the assumption of zero surface tractions is considered as a good approximation due to the large flat surface area of the liquid in the reservoir; (7) along the reservoir left wall GA, no slip velocity, i.e., $v_x = v_y = 0$.

Note that at point A there is a *singularity*, because mathematically the same node has a zero velocity if it belongs to the reservoir wall GA and a finite $V_R$ velocity if it belongs to the moving roll surface AB. Practically, there is a very small gap between the reservoir wall and the roll to allow for the roll motion. Numerically, we set very small elements around the corner node and set the corner node (point A) as a wall node (zero velocity) and the next node on the roll we set equal to the roll speed. This has been found to be the best way to handle the singularity (Mitsoulis et al., 1988; Loest et al., 1994), which otherwise may affect grossly the results (loss of mass flow rate).

In general, there are three *singularities* in this flow field: (a) at blade corner of point E, where the velocity is zero but the derivatives are discontinuous (zero-order singularity, flow around a corner wall); (b) at blade corner of point D, where the velocity is discontinuous changing *smoothly* from zero to a non-zero value due to the free surface (first-order singularity, flow at a solid/gas interface); and (c) at point A, where the wall meets a solid moving boundary and the velocity is discontinuous changing *abruptly* from zero to a distinct non-zero value (second-order singularity, flow from a non-moving to a moving boundary). This last one is the most severe and causes the most trouble numerically if not adequately handled.

For the simulations, all lengths have been made dimensionless by the minimum gap $H_0$, all velocities by the roll speed $V_R$, and all stresses and pressures by $\eta_0 V_R/H_0$.

## 3. METHOD OF SOLUTION

The above constitutive equation is solved together with the conservation equations under steady-state conditions using the Finite Element Method (FEM) with unknowns the velocities, pressures, and free surface coordinates (u-v-p-h formulation) (Mitsoulis et al., 1988). The finite elements used are 9-node Lagrangian quadrilateral isoparametric elements, with biquadratic interpolation functions for the velocity (u-v) and the free surface height (h), and bilinear functions for the pressure (p). Galerkin discretization is maintained for the integral terms of the governing equations and Gaussian quadrature is used for their integration. The numerical algorithm for convergence of the nonlinear system of the discretized algebraic equations is Picard iteration (direct substitution or fixed-point algorithm). Convergent solutions have been obtained independent of mesh size, provided enough elements are used in both the axial and vertical directions. The solution procedure for the Newtonian fluids reaches within 10 iterations machine accuracy for the norm-of-the-error of the updates (~$10^{-14}$), while the maximum difference in velocities is in the order of $10^{-4}$, in pressures around $10^{-3}$ and in change of free surface location around $10^{-8}$. For the shear-thinning Carreau



fluids, 120 iterations were used to reach slightly higher errors (~$10^{-6}$, $10^{-2}$, $10^{-1}$, $10^{-4}$, respectively). Unlike our previous experience with free-surface *viscoelastic* flows in extrusion (Barakos & Mitsoulis, 1995), it was not necessary to use under-relaxation for the free-surface movement. The dragging action of the moving roll was evidently responsible for bringing the free-surface movement to its final position without much effect from the stresses.

## 4. RESULTS AND DISCUSSION

The numerical simulations have been carried out for all 12 geometries used by Sullivan (1986) in his experimental design apparatus (see, e.g., figure 6 of Sullivan et al., 1987). It comprises the liquid reservoir with vertical walls, the channel between the blade and the roll, and the exit region, in an effort to compare the results with the experimental findings. The domain exit has been set to around 20 to 30$H_0$ from the channel exit, which was found sufficient to achieve a flat velocity profile with no further changes occurring.

***Table 2.*** *Different geometries used in blade-coating experiments by Sullivan (1986) and in the present simulations (R=6.985 cm, $V_R$=35 rpm = 25.6 cm/s).*

| W (cm) | ω (deg) | $H_0$ (cm) | Grid* | Grid Information (elem./nodes/dof**) |
|---|---|---|---|---|
| 1.313 | 0 | 0.1270 | L050 | 618/2631/4724 |
| 1.313 | 0 | 0.0762 | L030 | 570/2439/4388 |
| 1.313 | 0 | 0.0254 | L010 | 518/2225/4009 |
| 1.313 | 10 | 0.1270 | L1050 | 792/3341/5977 |
| 1.313 | 10 | 0.0762 | L1030 | 592/2523/4532 |
| 1.313 | 10 | 0.0254 | L1010 | 542/2325/4187 |
| 0.173 | 0 | 0.1270 | S050 | 656/2781/4985 |
| 0.173 | 0 | 0.0762 | S030 | 568/2421/4349 |
| 0.173 | 0 | 0.0254 | S010 | 572/2445/4397 |
| 0.173 | 10 | 0.1270 | S1050 | 656/2781/4985 |
| 0.173 | 10 | 0.0762 | S1030 | 560/2385/4283 |
| 0.173 | 10 | 0.0254 | S1010 | 572/2445/4397 |

* The grids are referred as L$\omega H_0$ or S$\omega H_0$, where L = large blade, S= small blade, ω = blade angle (deg) and $H_0$ = minimum height in mils (Sullivan, 1986).

** The degrees of freedom (dof) refer to the number of equations for velocities and pressures minus the number of known boundary conditions.

The calculations have been performed with several grids to establish results independent of mesh influence. Typical finite element grids have around 600 elements, 2500 nodes and 4500 degrees of freedom. All details regarding grid information and code names are given in table 2. Two typical grids are shown in figure 3 for large and small blades. Many elements are concentrated near the walls and the singularities (points A, D, and E of figure 1b), where most of the drastic changes occur.

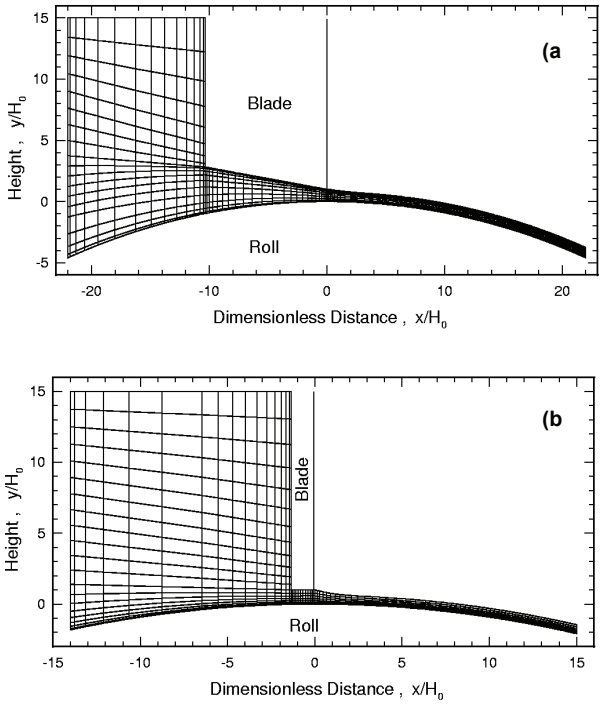


***Fig. 3.*** *Typical finite element grids used in the blade-coating simulations: (a) L1010 and (b) S050, see Table 2 for details.*

### 4.1. Coating thickness

Regarding coating thicknesses, all results are given in Table 3. It is seen that the shear-thinning fluids provide always thicker coatings than their Newtonian counterparts for the same geometry, by as little as 2.8% for S010 and as much as 10% for S1050. This finding is also predicted by the lubrication approximation theory (Sullivan, 1986). Our results are also in very good agreement with the results given by Sullivan et al. (1987) (see figure 4), although we have used different boundary conditions upstream. This is not surprising, because for purely viscous fluids as the ones considered here, the coating thickness depends on local variables and not on upstream kinematics and memory effects, as is the case for viscoelastic fluids (Mitsoulis & Triantafillopoulos, 1997; Mitsoulis & Pham, 1996).

In general, by keeping constant the geometric characteristics ($W$, $\omega$), an increase in the minimum gap $H_0$ causes an increase in the coating thickness $h$, and this conclusion is valid independent of the fluids used (Newtonian or Carreau). The influence of the blade angle ($\omega$) for constant ($W$, $H_0$) is to increase the coating thickness as well. Finally, the influence of the blade width ($W$) for constant ($\omega$, $H_0$) is to also



increase the coating thickness. The same conclusions have been reached by Sullivan et al. (1987).

***Table 3.*** *Coating thicknesses for different geometries used in blade-coating experiments by Sullivan (1986). Results from present simulations (R=6.985 cm, $V_R$=35 rpm = 25.6 cm/s).*

| Grid | $h^*= h / H_0$ | | h(mm) | | % Change |
|---|---|---|---|---|---|
| | Newtonian | Carreau | Newtonian | Carreau | |
| L010 | 0.675 | 0.720 | 0.171 | 0.183 | 7.018 |
| L030 | 0.641 | 0.672 | 0.488 | 0.512 | 4.918 |
| L050 | 0.622 | 0.652 | 0.790 | 0.828 | 4.810 |
| L1010 | 0.877 | 0.941 | 0.223 | 0.239 | 7.175 |
| L1030 | 0.810 | 0.861 | 0.617 | 0.656 | 6.321 |
| L1050 | 0.765 | 0.828 | 0.972 | 1.052 | 8.230 |
| S010 | 0.566 | 0.583 | 0.144 | 0.148 | 2.778 |
| S030 | 0.585 | 0.632 | 0.446 | 0.482 | 8.072 |
| S050 | 0.608 | 0.660 | 0.772 | 0.838 | 8.549 |
| S1010 | 0.744 | 0.789 | 0.189 | 0.200 | 5.820 |
| S1030 | 0.697 | 0.759 | 0.531 | 0.578 | 8.851 |
| S1050 | 0.678 | 0.745 | 0.861 | 0.946 | 9.872 |

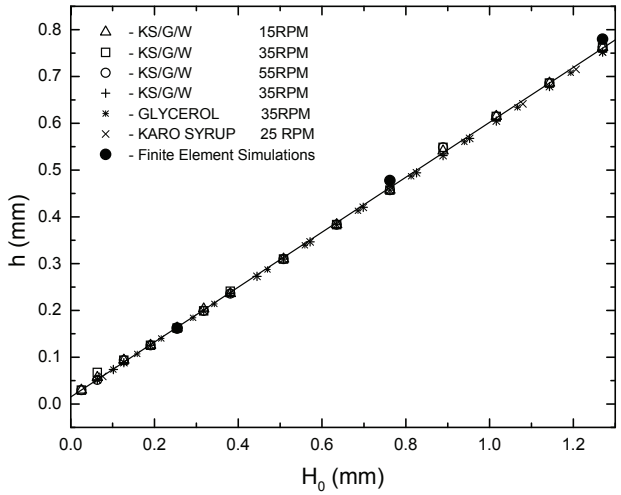


***Fig. 4.*** *Coating thickness as a function of minimum gap $H_0$ for Newtonian fluids. Experimental results by Sullivan [2] and current numerical simulations by the Finite Element Method. The abbreviations are: KS=Karo Syrup, G=Glycerol, W=water.*

***Table 4.*** *Coating thicknesses for different roll speeds used in blade coating. Results from present simulations (R = 6.985 cm, L010).*

| Roll Speed $V_R$ (rpm) | $h^*= h / H_0$ | | h(mm) | |
|---|---|---|---|---|
| | Newtonian | Carreau | Newtonian | Carreau |
| 35 | 0.675 | 0.720 | 0.171 | 0.183 |
| 350 | 0.675 | 0.706 | 0.171 | 0.179 |

Changing the roll speed by an order-of-magnitude (i.e. from 35 rpm to 350 rpm) gives no changes in the coating thickness for the Newtonian fluids as expected from dimensionless arguments, while for the shear-thinning Carreau fluid there is a slight decrease in the order of 2% for a given geometry (L010). The results are given in table 4 for this case and are again in agreement with the experimental observations by Sullivan (1986).

## 4.2. Upstream kinematics

A major part of this work is dealing with the streamline patterns that exist upstream of the blade in any coating operation, due to the dragging action of the roll or a moving web (Davard & Dupuis, 2000). We begin with a typical streamline pattern corresponding to the geometry of L1030 for a Newtonian and a shear-thinning fluid modelled by the Carreau equation (4). As shown in figure 5, there are big vortices in both cases, but in a dimensionless form the vortex for the shear-thinning fluid is much less in size and intensity than its Newtonian counterpart.

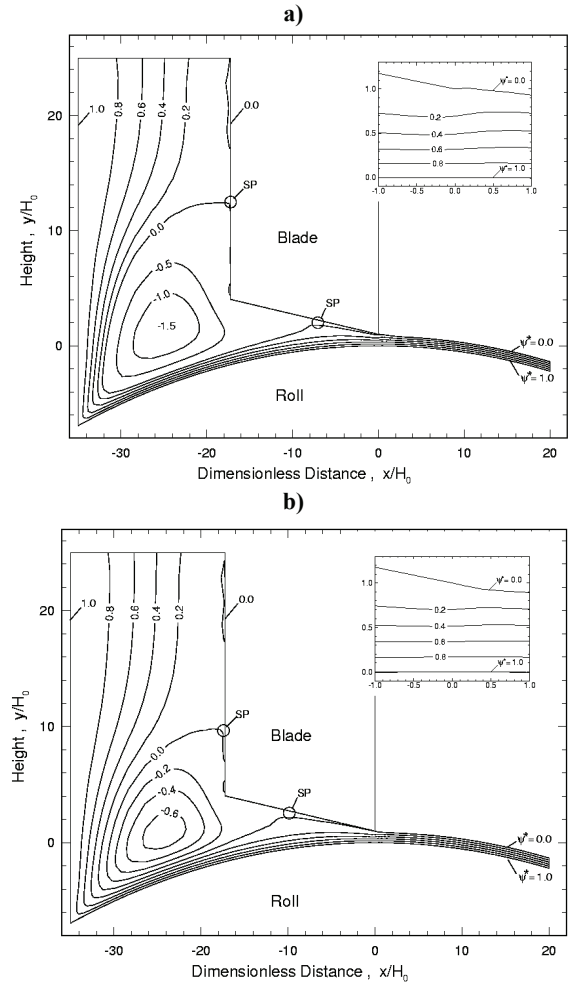


***Fig. 5.*** *Streamline patterns for (a) Newtonian and (b) Carreau fluid in the L1030 geometry. The inset shows details near the blade exit where the free surface starts.*

The vortex intensity is determined by the dimensionless value of the stream function $\psi^*_{v,\min}$ in the



eye of the vortex. The stream function is made dimensionless and normalized according to the following formula

$$\psi^* = \frac{\psi - \psi_C}{\psi_B - \psi_C} \qquad (6)$$

where $\psi_B$ is the value of the stream function on the roll surface (or point B of figure 1b), and $\psi_C$ is the value of the stream function on the free surface (or point C of figure 1b). In such a way, the denominator $\psi_B$ - $\psi_C$ corresponds to the flow rate that leaves the flow field, and in normalized form takes the value of 1. The zero value of the normalized stream function determines the separating streamline and sets the vortex envelope. Then, the value of $\psi^*_{v,\min}$ in the eye of the vortex corresponds to the amount of flow rate that recirculates in the vortex envelope.

With the above definitions and referring to figure 5, it is seen that about 150% of the Newtonian fluid recirculates in the reservoir, while only about 60% of the shear-thinning fluid recirculate. This is in agreement with the shear-rate dependence of the viscosity, which makes the fluid more difficult to move in regions of low shearing, as is the case in the vortex area.

Another interesting feature is the appearance of the two *stagnation points* (denoted as SP in the figures), where the zero-streamline hits the blade wall. These are the points where the flow splits into two and where the shear stress becomes zero. Their exact location can be found by plotting the shear stress profile as a function of the dimensionless axial distance *x/H0*, as shown in figure 6. The *singularities* at the blade corners (points D and E of figure 1b, shown as dashed lines here) are responsible for creating the high stress jumps, due to the abrupt changes in the velocity (point D) and its gradient (point E).

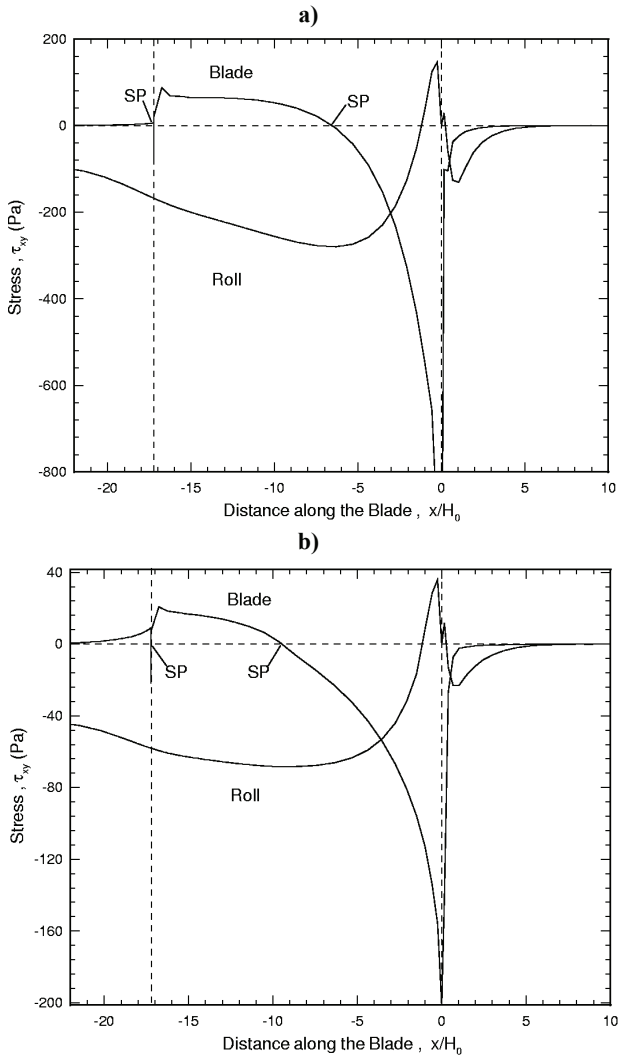


***Fig. 6.*** *Axial shear stress profiles along the blade wall and the roll for (a) Newtonian and (b) Carreau fluid in the L1030 geometry. The dashed lines correspond to the corners of the blade (singular points D and E of Fig. 1b).*

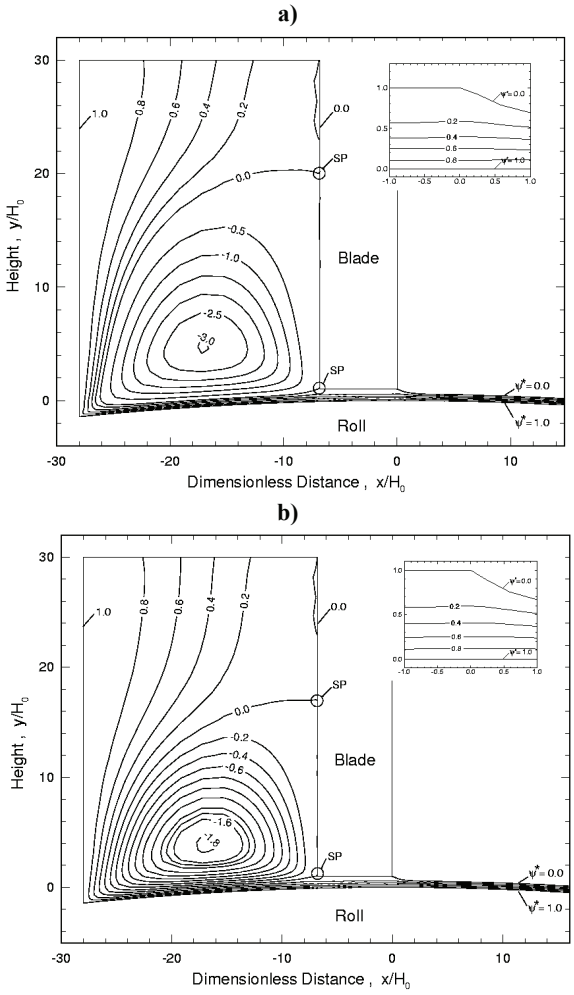


***Fig. 7.*** *Streamline patterns for (a) Newtonian and (b) Carreau fluid in the S010 geometry. The inset shows details near the blade exit where the free surface starts.*



Another interesting case is the geometry S010, which gives the streamline patterns of figure 7 for the two fluids. The Newtonian fluid recirculates 300% of the flow rate, while the Carreau fluid recirculates 180% of the flow rate in this geometry. The stagnation points SP in this geometry (and all other small blade geometries) are on the vertical blade wall ending at the blade corner, and thus the vortex does not reach under the blade. The corresponding stresses show this as well, as evidenced in figure 8. The values of the shear stresses are also much lower than the Newtonian ones due to shear thinning.

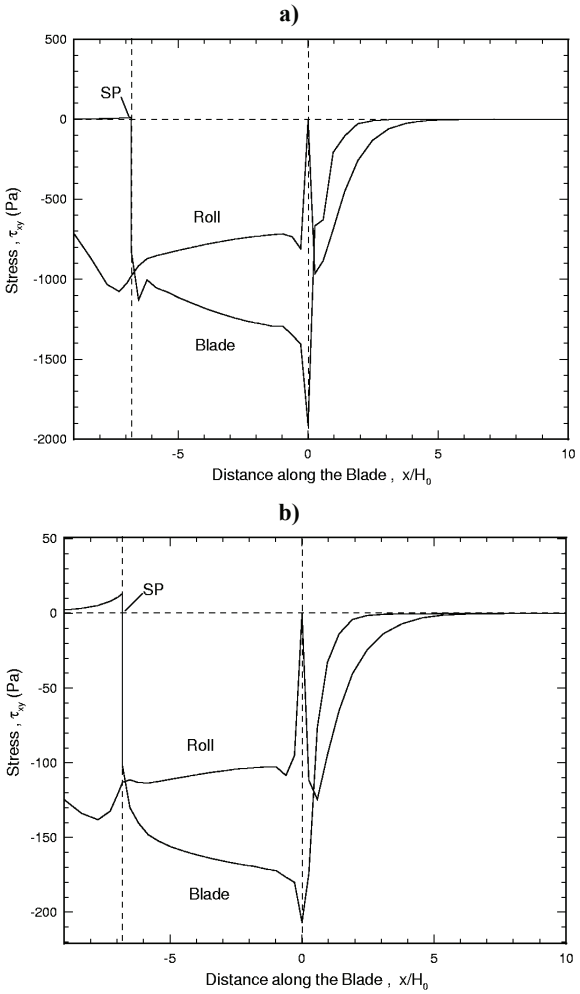


***Fig. 8.*** *Axial shear stress profiles along the blade wall and the roll for (a) Newtonian and (b) Carreau fluid in the S010 geometry. The dashed lines correspond to the corners of the blade (singular points D and E of Fig. 1b).*

It is instructive to change the geometry of the upstream reservoir and see what changes are affected in the flow field. We have used as reference the L1010 geometry and the Carreau model. First, we have changed the height of the reservoir and observe no change whatsoever in vortex size and intensity (see figure 9b). Then, we have changed the width of the reservoir, and here we observe a change in the vortex intensity and in the location of the

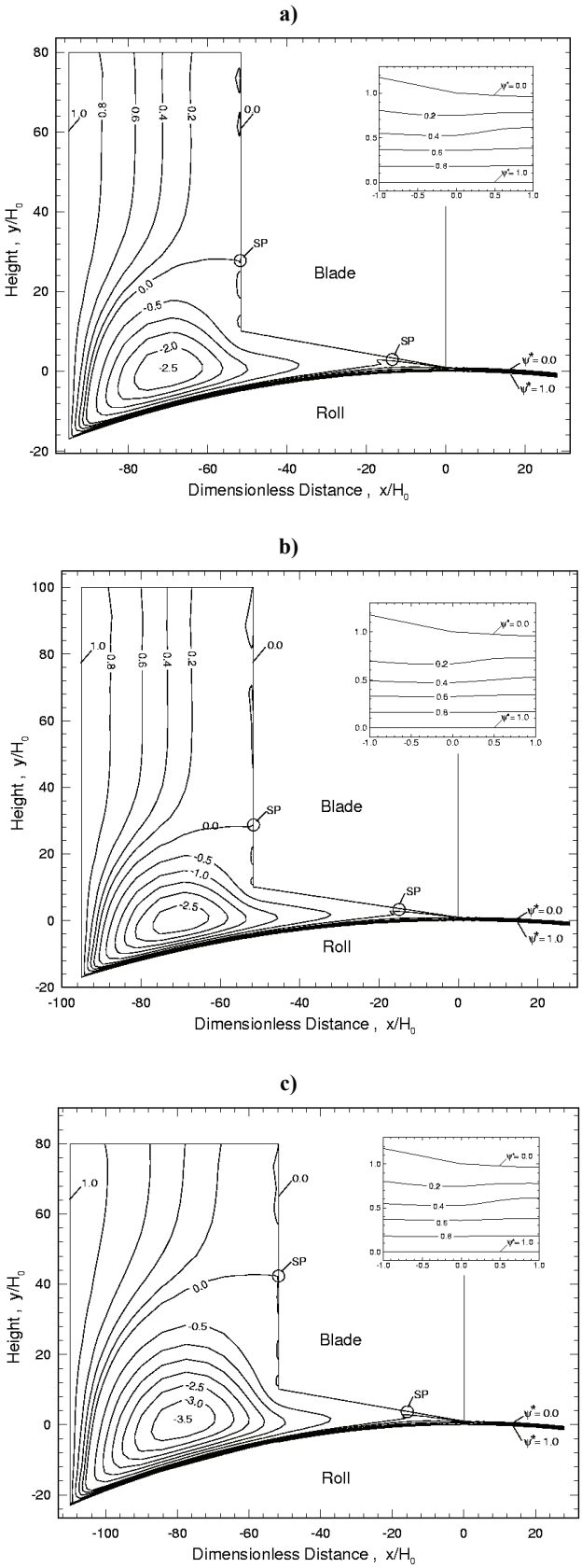


***Fig. 9.*** *Influence of reservoir geometry on the streamline patterns for a shear-thinning Carreau fluid: (a) original design, (b) design with higher reservoir walls, (c) design with wider reservoir walls. The inset shows details near the blade exit where the free surface starts.*



stagnation point on the vertical blade wall to accommodate the bigger flow field. However, the location of the stagnation point under the blade is not affected nor was the coating thickness. Therefore, we conclude that for viscous shear-thinning fluids, the changes in the reservoir size affect only the amount of recirculating vortices but not the coating thickness nor the location of the stagnation point under the blade.

### 4.3. Pressure and stresses

The numerical simulation gives also a wealth of information about the pressure and normal stresses in the flow field. A typical example of isobars and pressure distribution under the blade and on the roll surface is given in figure 10 for the Carreau model in the L1010 geometry. The isobars have been made dimensionless and normalized with the maximum and minimum values of the pressure, according to the formula

$$P^* = \frac{P - P_{\min}}{P_{\max} - P_{\min}} \qquad (7)$$

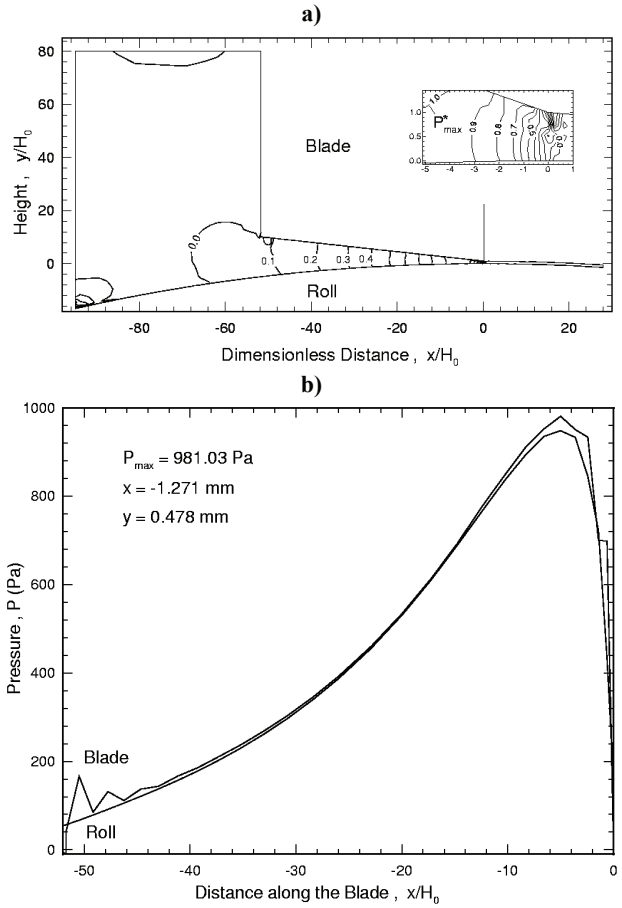


***Fig. 10.*** *(a) Isobars and (b) pressure distribution in blade coating of a shear-thinning fluid obeying the Carreau model in the L1010 geometry. The inset shows details near the blade exit where the free surface starts.*

where $P_{max}$ and $P_{min}$ are the maximum and minimum pressures in the field, respectively. The value of the maximum pressure is given in figure 10b together with the coordinates of its location. We observe that due to the severe singularities at points A and C of figure 1b, the isobars are dense there (see inset for details near the blade exit).

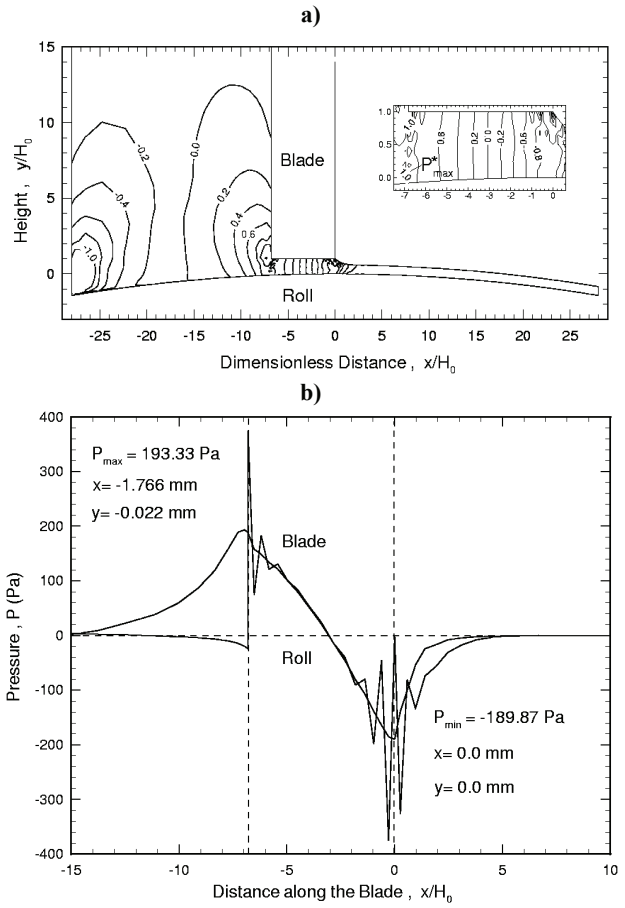


***Fig. 11.*** *(a) Isobars and (b) pressure distribution in blade coating of a shear-thinning fluid obeying the Carreau model in the S010 geometry. The inset shows details near the blade exit where the free surface starts.*

The pressure distributions are almost the same under the blade and on the roll surface, but due to the small angle they are not identical. This is the case for the flat blades, where the lubrication approximation is exactly valid. An example of this is given in figure 11b for the S010 geometry. In this figure, the singularities at the blade corners (points D and E of figure 1b) cause the sharp spikes for the pressure, but on the smooth roll surface the pressure distribution is also smooth. The pressure distributions for the two surfaces coincide in the middle region under the blade due to the flat blade used. The results for the pressure distribution also make clear that this geometry is not as good as others, because of the negative pressures generated in the field under the blade. It is, therefore, necessary to



have a big enough blade to generate enough pressure in the flow field for a certain roll speed.

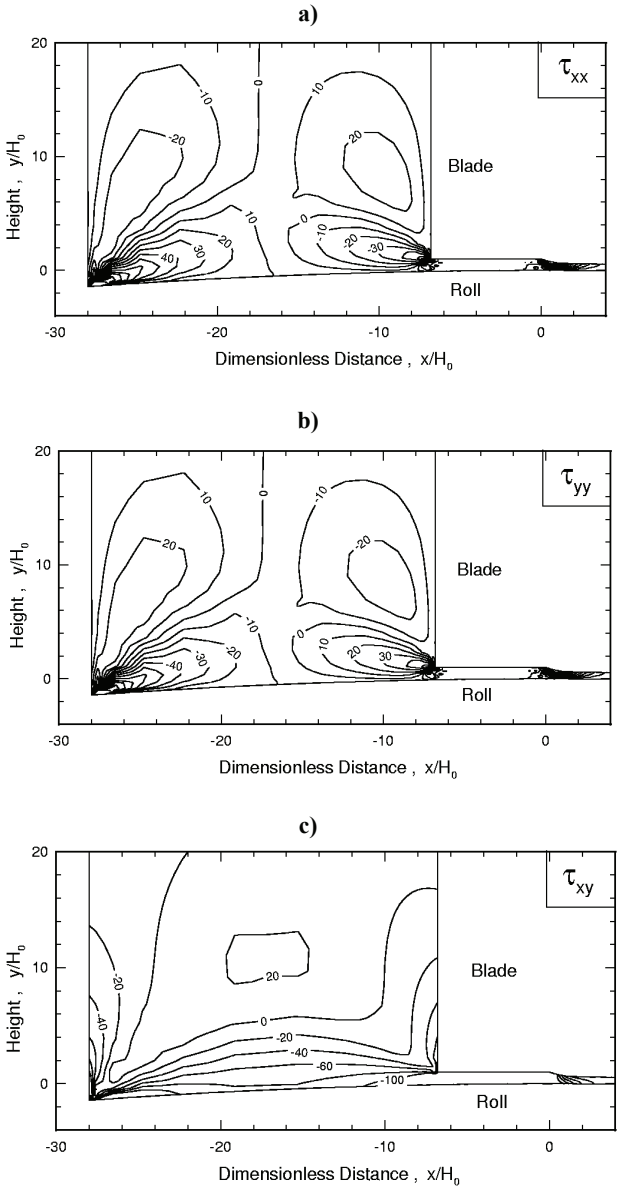


***Fig. 12.*** *Stress contours in blade coating of a shear-thinning fluid obeying the Carreau model in the S010 geometry: (a) $\tau_{xx}$, (b) $\tau_{yy}$, (c) shear stress $\tau_{xy}$.*

Finally, a typical example of the stress contours is given in figure 12, for the three stresses (normal stresses $\tau_{xx}$, $\tau_{yy}$ and shear stress $\tau_{xy}$) in the S010 geometry. This type of information can be useful in determining the maximum absolute values of stresses that the fluid is subjected to and which may be detrimental to the coating if exceeded.

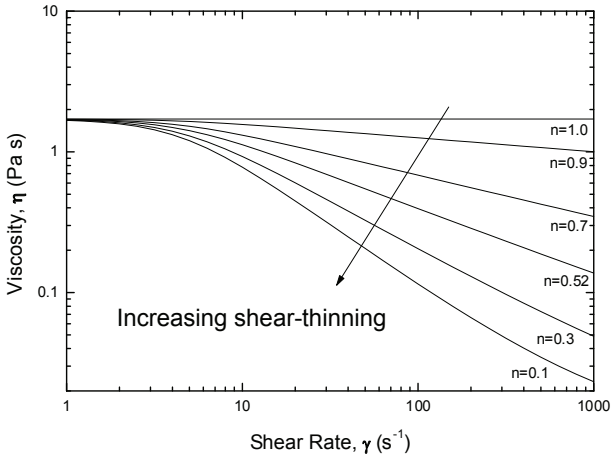


***Fig. 13.*** *Shear viscosity as a function of shear rate predicted by the Carreau model for different values of the power-law index n.*

### 4.4. Parametric study of power-law index *n*

In an effort to understand the influence of shear-thinning behaviour on the coating thickness and streamline patterns, we have undertaken a parametric study of the power-law index $n$ in the Carreau model (eq. 4) between the values of $n = 1$ (Newtonian fluid) and $n = 0$ (extreme shear thinning). The viscosity behaviour for select $n$ values is given in figure 13 for the Carreau model that describes the shear-thinning behaviour of the CMC aqueous polymer solution.

The results for the coating thickness are given in figure 14 for the select geometry L010. We observe the very interesting phenomenon of coating thickness increase for $n > 0.3$, after which there is a decrease all the way to $n = 0$. This behaviour is similar to results in other geometries, such as extrudate swell of power-law fluids (Mitsoulis et al., 1984) and in the calculation of the drag coefficient in flow of power-law fluids around a sphere (Missirlis et al., 2001).

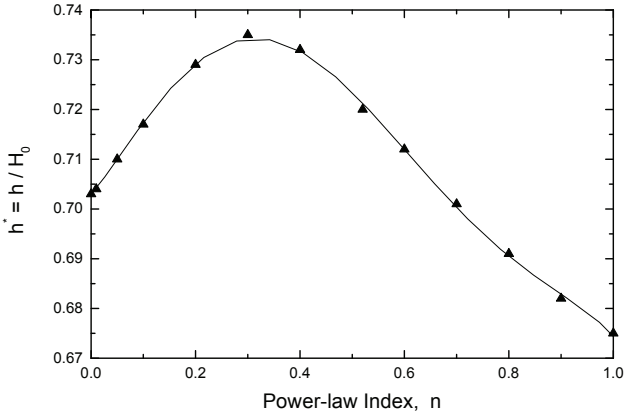


***Fig. 14.*** *Coating thickness as a function of the power-law index n in blade-coating simulations with the Carreau model in the L010 geometry.*



The corresponding results for the vortex intensity are given in figure 15, where it is seen that a monotonic linear decrease in the amount of recirculation is obtained as the power-law index goes from a Newtonian behaviour to an extreme shear-thinning one. This linear decrease is valid for all geometries, but the amount of recirculation depends on each geometry considered.

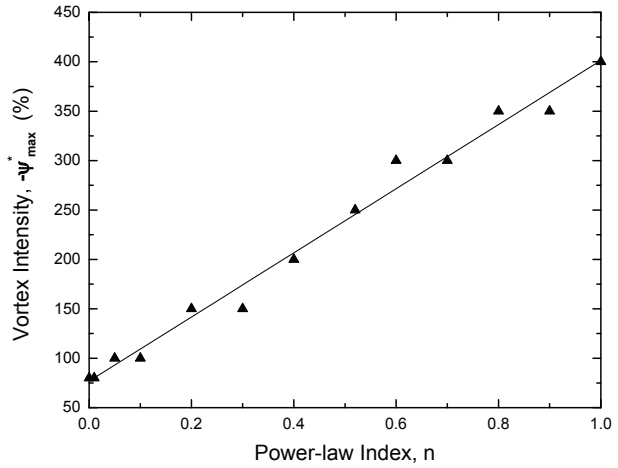


***Fig. 15.*** *Percent recirculation as a function of the power-law index n in blade-coating simulations with the Carreau model in the L010 geometry.*

## 5. SUMMARY

The process of blade-over-roll coating has been simulated numerically as a fully two-dimensional, steady-state, isothermal flow using the finite-element method. Newtonian and shear-thinning fluids are considered, the latter being modeled with the Carreau constitutive equation. The simulations have been carried in 12 different geometries, taking into account the reservoir wall upstream of the blade. Its presence affects the vortex size and intensity but not the final coating thickness, which depends for viscous fluids both on the blade geometry and the rheology (amount of shear thinning) of the coating fluid.

It was found that opening the minimum gap, opening the blade angle and making the blade larger increase the coating thickness, which was also found previously experimentally. More shear-thinning also increases the coating thickness for values of the power-law index $n$ down to 0.3, after which a decrease is observed. The amount of recirculation in the reservoir decreases monotonically with an increase in shear thinning (i.e., a decrease in the power-law index $n$).

The present results show that for purely viscous fluids there is now a good way of obtaining accurate predictions and details of the flow field, despite the many difficulties of the coating flows (existence of stagnation points, free surfaces, and singularities of varying degree of difficulty). This is a good starting point for the much more demanding and harder task of simulating viscoelastic coating flows, where the problem is compounded by the choice of a proper constitutive equation and the numerical handling of singularities and recirculating patterns.

## ACKNOWLEDGEMENTS

Financial assistance from the National Technical University of Athens (NTUA) is gratefully acknowledged.

## REFERENCES

Barakos, G., Mitsoulis, E., 1995, Numerical simulation of extrusion through orifice dies and prediction of Bagley correction for an IUPAC-LDPE melt, *J. Rheol.*, 39, 193-209.

Davard, F., Dupuis, D., 2000, Flow visualization experiments in a blade coating process, *J. Non-Newtonian Fluid Mech.*, 93, 17-28.

Kistler, S.F., Scriven, L.E., 1984, Coating flow theory by finite element and asymptotic analysis of the Navier-Stokes system, *Int. J. Num. Meth. Fluids*, 4, 207-229.

Loest, H., Lipp, R., Mitsoulis, E., 1994, Numerical flow simulation of viscoplastic slurries and design criteria for a tape casting unit, *J. Amer. Ceram. Soc.*, 77, 254-262.

Missirlis, K.A., Assimacopoulos, D., Mitsoulis, E., Chhabra, R.P., 2001, Wall effects for motion of spheres in power-law fluids, *J. Non-Newtonian Fluid Mech.*, 96, 459-471.

Mitsoulis, E., 1990, Numerical simulation of viscoelastic fluids, in *Encyclopedia of Fluid Mechanics, 9, Polymer Flow Engineering*, ed., Cheremisinoff, N.P., Gulf Publ. Co., Dallas, Texas, USA, 649-704.

Mitsoulis, E., Pham, T.V., 1996, Numerical simulation of rheological effects in blade coating flows*, Proceedings of XIIth International Congress on Rheology*, eds, Ait-Kadi, A., Dealy, J.M., James, D.F., Williams, M.C., Chem. Eng. Dept., Univ. Laval, Quebec City, CANADA, 423-424.

Mitsoulis, E., Triantafillopoulos, N., 1997, Viscoelasticity in blade coating of non-Newtonian fluids*, Proceedings of the 1997 TAPPI Advanced Coating Fundamentals Symposium*, Philadelphia, PA, USA, 27-41.

Mitsoulis, E., Vlachopoulos, J., Mirza, F.A., 1984, Numerical simulation of entry and exit flows in slit dies, *Polym. Eng. Sci.*, 24, 707-715.

Mitsoulis, E., Wagner, R., Heng, F.L., 1988, Numerical simulation of wire-coating low-density polyethylene: theory and experiments, *Polym. Eng. Sci.*, 28, 291-310.

Sullivan, T., *An Experimental and Computational Investigation of Rheological Effects in Blade Coating*, PhD Thesis, University of California, San Diego, CA, USA.

Sullivan, T., Middleman, S., 1986, Film thickness in blade coating of viscous and viscoelastic liquids, *J. Non-Newtonian Fluid Mech.*, 21, 13-38.



Sullivan, T., Middleman, S., Keunings, R., 1987, Use of a finite-element method to interpret rheological effects in blade coating, *AIChE J.*, 33, 2047-2056.

## MODEL CIEPLNY PROCESU ŁĄCZENIA TARCIOWEGO Z MIESZANIEM MATERIAŁU ZGRZEINY NA PRZYKŁADZIE STOPU Al-Zn-Mg-Cu MODYFIKOWANEGO SKANDEM

Streszczenie

Niewielki dodatek skandu do stopu Al-Zn-Mg-Cu z serii 7000 może w znaczący sposób poprawić właściwości mechaniczne w temperaturze pokojowej oraz powstrzymać spadek wytrzymałości w temperaturze podwyższonej. W zaprezentowanych badaniach dokonano oceny właściwości mechanicznych połączeń stopu Al-Zn-Mg-Cu modyfikowanego skandem wykonanych metodą zgrzewania tarciowego z mieszaniem materialu zgrzeiny (FSW). Badania mechaniczne wykonano na materiale rodzimym oraz na próbkach zgrzewanych z prędkościami obrotowymi narzędzia 175, 225, 250, 300, 350 i 400 obrotów na minutę (przy jednakowych pozostałych parametrach procesu). Opracowano komputerowy model cieplny zgrzewania tarciowego z mieszaniem materiału zgrzeiny wykorzystujący energetyczny współczynnik ujmujący poślizg narzędzia w trakcie procesu. Współczynnik ten zaproponowano w oparciu o doświadczalną zależność pomiędzy stosunkiem maksymalnej temperatury podczas zgrzewania do temperatury solidus oraz energii wydatkowanej na jednostkę długości zgrzeiny. Opracowany model bardzo dobrze przewiduje maksymalne temperatury zgrzewania dla szerokiego zakresu energii oraz wykazuje dobrą korelację właściwości mechanicznych z temperaturą przewidzianą przez model.

*Received: December 20, 2009*
*Received in a revised form: May 20, 2010*
*Accepted: June 14, 2010*